Interband Faraday and Kerr rotation and magnetization of $Pb_{1-x}Eu_xTe$ in the concentration range $0<x\leqslant 1$

H. Krenn
Institut für Halbleiter- und Festkörperphysik, Universität Linz, A-4040 Linz, Austria

W. Herbst and H. Pascher
Experimentalphysik I, Universität Bayreuth, D-95440 Bayreuth, Germany

Y. Ueta,* G. Springholz, and G. Bauer
Institut für Halbleiter- und Festkörperphysik, Universität Linz, A-4040 Linz, Austria
(Received 16 November 1998; revised manuscript received 22 February 1999)

Faraday and magneto-optical Kerr effect has been used for the investigation of the band alignment as well as of the magnetic properties of epitaxial layers of the ternary alloy system $Pb_{1-x}Eu_xTe$ ($0\leqslant x\leqslant 1$) grown on BaF_2 substrates. Due to the wide range of transition energies ($0.19\,eV\leqslant E_g\leqslant 2.25\,eV$) the experiments had to be performed in the spectral range from midinfrared to visible light. Data were collected at temperatures between 1.8 and 250 K and in magnetic fields up to 7 T. Concomitant magnetization measurements ($B=1$ T) were performed with a superconducting quantum interference device (SQUID) magnetometer and compared with measurements of the x dependence of the Verdet constant. The variation of the fundamental absorption gap with Eu content can be understood in terms of the relative energetic position of PbTe-related band edges and Eu $4f$ and $5d$ levels: $\Delta E_g/\Delta x=4.48$ eV for $x<0.06$; $\Delta E_g/\Delta x=2.03$ eV for $0.06<x<0.6$. For $x>0.8$, the electronic transitions are identified to be EuTe-like. The most striking feature is a sign reversal of Verdet's constant around $x=0.15$, which is attributed to a crossover of Faraday rotation caused by band electrons (holes) and interacting pairs of magnetic ions and a metal-insulator transition. An antiferromagnetic phase transition is observed for $x>0.8$ in magneto-optics as well as in SQUID magnetometry.
[S0163-1829(99)03235-X]

I. INTRODUCTION

The ternary system $Pb_{1-x}Eu_xTe$ (Refs. 1 and 2) is a semiconductor whose alloy constituent Europium (Eu) tunes the fundamental absorption gap over a wide-energy range from $E_g=0.334$ eV ($T=300$ K) for PbTe to $E_g=2.25$ eV for EuTe. Both PbTe and EuTe crystallize in the NaCl lattice structure and are (as bulk crystals) completely miscible over the entire concentration range. It is a common property of the magnetic elements Eu and Mn that they provide a large tunability of the energy gaps even for low concentrations in PbTe, which has been used in midinfrared laser applications.[3–6]

$Pb_{1-x}Eu_xTe$ has been investigated by magnetooptics only in the low concentration range ($x<0.06$).[7] The analysis of magnetization[8–10] ($x\leqslant 0.32$) and of magnetization steps[11] ($x\leqslant 0.06$) in high-magnetic fields has given information about the distribution of Eu atoms and their mutual magnetic exchange interaction. The electronic band structure and the magnetooptical properties of the binary material PbTe are well known.[12–14] For EuTe the magnetization and band structure near the fundamental absorption has been determined long time ago.[15–19] Detailed band-structure calculations are only available for the related Eu chalcogenides (EuO, EuS, EuSe).[20]

In EuTe, the uncompensated $4f$ spins of the Eu atoms (total spin $S=\frac{7}{2}$) form a three-dimensional Heisenberg spin lattice with antiferromagnetic ordering below $T_N=9.6$ K. In fact, EuTe is one of the most prominent representatives of a Heisenberg antiferromagnet[21–23] with a very local-magnetic moment and short-range Eu-Eu exchange interaction.

Only little information about the band and magnetic properties is available in the intermediate concentration range ($0.1<x<0.9$) of the alloy system $Pb_{1-x}Eu_xTe$. Since the band arrangements are quite different for low and high-Eu contents (as known from the binaries PbTe, EuTe), magnetooptical investigations are of particular importance in the intermediate concentration range. In addition, the magnetic ordering of this alloy system is also influenced by the change of band structure, and the transition from the paramagnetic behavior for the dilute alloy to the long-range antiferromagnetic order for the high concentrations has to be investigated.

In the present paper, we shall concentrate ourselves on the evaluation of magnetooptic Faraday rotation and magnetooptic Kerr effect (MOKE) spectra of $Pb_{1-x}Eu_xTe$ in the absorbing regime ($\hbar\omega=E\geqslant E_g$) as well as below the fundamental band gap ($\hbar\omega=E<E_g$). Since Faraday rotation and MOKE are inherent differential techniques (they measure the *phase differences* of right- and left-hand circularly polarized transmission or reflection, respectively) the dynamic range of the measurement is substantially increased. Magnetotransmission or magnetoreflection are alternative techniques that allow an accurate determination of the *fundamental* energy gap (the energetically lowest absorbing transition). They are less suitable to recover absorption features far above the fundamental absorption, unless modulation methods like photo-, electro-, or piezomodulated reflectance are used.

In mixed systems as in $Pb_{1-x}Eu_xTe$ (x being the intermediate concentration range) absorption features may originate from PbTe-like as well EuTe-like transitions. The system with the lower absorption energy (PbTe) could mask the absorption of the higher transition energy (EuTe). However, EuTe is a magnetic semiconductor, thus, we expect an enhanced Faraday rotation in the strongly absorbing regime under the presence of magnetized Eu ions. Hence, the magnetooptical method could be superior to the cited conventional techniques.

Concomitant magnetization measurements using a superconducting quantum interference device (SQUID) are compared with the (linear) Faraday- and MOKE experiments, to prove the question whether the specific angle-rotation (the so-called Verdet constant) scales with magnetization, measured by the SQUID. Indeed, it will be shown that the magnetization state of a sample as probed by Faraday rotation, can be different from the one measured by magnetometry. To sustain the original magnetic structure during the investigations a rather low-magnetic field is applied ($B=0.5$ T for Faraday and Kerr rotation, $B=1$ T for SQUID). In addition, Faraday rotation experiments were performed for a magnetic field towards the saturation field[24] (7.2 T at 1.8 K) of EuTe to demonstrate the crossover from the antiferromagnetic to the paramagnetic phase.

After the introduction (Sec. I), Sec. II of the paper presents the theory of interband Faraday rotation to an extent that is important for discussing the results. Section III gives information about the experiments. Sample preparation is also described in Sec. III. Faraday rotation and MOKE spectra are presented in Sec. IV together with magnetization data. Since the mixed system $Pb_{1-x}Eu_xTe$ covers a wide spectral range, optical investigations to identify the magnetic interactions have to be performed from the midinfrared to the visible. The narrow-gap semiconductors exhibit a relatively high concentration of free carriers ($4\times10^{17}\,\mathrm{cm}^{-3}$), whereas the wide-gap materials are semi-insulating. In the former class the carrier-/magnetic-ion exchange interaction will be dominant, and the characteristics of the nonmagnetic host semiconductor electronic band structure governs the exchange mechanism. At higher concentrations ($x>0.1$) the indirect exchange interaction between the magnetic centers themselves comes into play. So far, the x value required for the onset of a cooperative phase transition was still under question to the best of our knowledge.

An observed sign change of the Verdet constant as a function of Eu content is discussed in terms of magnetic interactions between magnetic ions and a recently discovered metal-insulator transition (MIT) in $Pb_{1-x}Eu_xTe$.[25] In Sec. V, we shall discuss the resonant and nonresonant interband Faraday and MOKE rotation spectra in the context with magnetization data measured by the SQUID. Section VI presents the conclusions of our work.

II. THEORY OF RESONANT AND NONRESONANT INTERBAND FARADAY ROTATION

In the following, a general expression for the specific Faraday rotation angle (Verdet's constant) is derived and connected with the magnetization of a diluted magnetic semiconductor. In Faraday configuration in which the magnetic field $\mathbf{B}=(0,0,B)$ is applied along the propagation direction of the electromagnetic wave of frequency ω (photon energy $E=\hbar\omega$), the Faraday rotation angle $\theta_F(E)$ for an optically isotropic medium of thickness d is given by[26]

$$\theta_F(E)=\frac{\omega d}{2c}[n_+(E)-n_-(E)]\approx\frac{\omega d}{4nc}[n_+^2(E)-n_-^2(E)]$$

$$=\frac{\omega d}{4nc}[\hat{\varepsilon}_+(E)-\hat{\varepsilon}_-(E)]. \tag{1}$$

In Eq. (1), c is the velocity of light in vacuum, and $n_\pm=\sqrt{\varepsilon_{xx}\pm i\varepsilon_{xy}}$ are the refractive indices for the two counterrotating circular polarizations of light, induced by off-diagonal terms $\varepsilon_{xy}=-\varepsilon_{yx}$ of the dielectric tensor. An optically inactive medium is described by diagonal terms of this tensor, which gets nondiagonal only in the presence of an external magnetic field, or due to a symmetry break from spontaneous magnetization of the medium. In general, the refractive indices are complex, and the rotation angle possesses also an imaginary part: This means that the polarization of light gets not only rotated, but becomes also elliptic. The latter reflects an unbalanced absorption of right- and left-hand circularly polarized light (*circular dichroism*). In Eq. (1) we used the approximation

$$(n_+-n_-)=(n_+^2-n_-^2)/(n_++n_-)\approx(n_+^2-n_-^2)/2n,$$

where it is assumed that the mean index of refraction (n) for both polarizations corresponds to the case without magnetic field or magnetization. From selection rules of electronic transitions between orbital or band states it is well known that electric dipole allowed transitions connect states of different parity, and circularly polarized excitations are governed by the $\varepsilon_\pm=\varepsilon_{xx}\pm i\varepsilon_{xy}$ contributions to the dielectric function. Thus, the rotation angle of Eq. (1) reflects the nondiagonal part of the dielectric function, which in turn is nonzero in a nonvanishing magnetic field or magnetization. We notice that by this relationship the magnetization state of a sample can be probed by examining optically induced electronic transitions, but the mechanism of coupling between electrons and magnetic centers must be known in advance. For an interband transition between a valence (v) and conduction (c) band the standard expression of the imaginary part of the dielectric function for dipole allowed transitions is given by[27]

$$\mathrm{Im}\,\hat{\varepsilon}_\pm=\frac{\pi e^2\hbar^2}{\varepsilon_0 m_0^2}\frac{1}{E^2}g_{cv}^{\pm}(E)|\langle p_{cv}^{\pm}\rangle|^2. \tag{2}$$

The constants in the prefactor of Eq. (2) are the charge and mass (e,m_0) of an electron, Planck's constant ($\hbar=h/2\pi$) and the permittivity of vacuum (ε_0). The selection rule for circularly polarized excitation ($\pm$) manifests itself in a nonvanishing momentum matrix element $\langle p_{cv}^{\pm}\rangle=\langle c|\overline{p}\cdot\overline{e^{\pm}}|v\rangle$ for a light-polarization unit vector $\overline{e^{\pm}}=(e_x,\pm ie_y,0)/\sqrt{2}$. The joint density of states $g_{cv}^{\pm}(E)$ is the number of possible transition channels per spin-split state ($\pm$) for a given photon energy E within unit energy interval. Since we are interested in the rotation angle, the real part of the dielectric function is of importance for evaluating $\theta_F(E)$ according to Eq. (1). We obtain $\mathrm{Re}(\varepsilon)$ by a Kramers-Kronig transformation of $\mathrm{Im}(\varepsilon)$

$$\mathrm{Re}[\varepsilon(E)]=\frac{2}{\pi}\int_0^\infty \frac{E'\,\mathrm{Im}[\hat{\varepsilon}(E')]}{E'^2-E^2}\,dE'. \tag{3}$$

The most prominent feature of $\mathrm{Im}(\hat{\varepsilon})$ is related with the fundamental absorption. For PbTe the direct energy gap E_g is located at the L point of the Brillouin zone with a considerable anisotropy of effective masses $M_\parallel$, $M_\perp$ parallel ($\parallel$) and perpendicular ($\perp$) to the [111] direction of the L-point wave vector. For $Pb_{1-x}Eu_xTe$ ($x<0.1$), we treat the nonparabolic band structure of the IV-VI host semiconductor (PbTe) within a simple two-band model taking into account only the L_6^--conduction and the L_6^+-valence band including far-band corrections to the effective band-edge masses $M_\perp$, $M_\parallel$. We obtain for the joint density of states in zero-magnetic field[27,28]

$$g_{cv}^{\pm}(E)=\frac{M_\perp\sqrt{M_\parallel}}{2\pi^2\hbar^3E_{\sigma^\pm}^{3/2}}E(E^2-E_{\sigma^\pm}^2)^{1/2}. \tag{4}$$

Equation (4) holds for a single valley at the L point of the Brillouin zone. $E_{\sigma^\pm}$ are the spin-split interband gap energies for the carrier spins aligned parallel (+) and antiparallel (−) to the magnetic field. The spin-splitting ΔE of the transition energy gap E_g is

$$\Delta E=E_{\sigma^+}-E_{\sigma^-},$$

$$E_{\sigma^\pm}=E_g\pm\Delta E/2. \tag{5}$$

To get the total joint density of states (JDOS) over all valleys, Eq. (4) has to be multiplied by the valley degeneracy factor $g_v=4$. Following the procedure of Ref. 27 [Eqs. (20)–(25)] we calculate the real part of the dielectric function using the Kramers-Kronig transformation Eq. (3) and the JDOS of Eq. (4) to obtain

$$\mathrm{Re}[\hat{\varepsilon}_\pm(E)]=\varepsilon_\infty-\frac{2A}{\pi}\frac{(E^2-E_{\sigma^\pm}^2)^{1/2}}{E}\tanh^{-1}\left[\frac{E}{(E^2-E_{\sigma^\pm}^2)^{1/2}}\right]. \tag{6}$$

The dimensionless parameter A is interpreted as the near-band-gap oscillator strength (using the transverse and longitudinal interband momentum-matrix elements $P_\perp$, $P_\parallel$ at the L point of the Brillouin zone)

$$A=\frac{g_\nu e^2}{\pi\varepsilon_0 m_0^2\hbar}\frac{M_\perp\sqrt{M_\parallel}}{E_\sigma^{3/2}}\frac{2P_\perp^2+P_\parallel^2}{3}. \tag{7}$$

In order to estimate the magnetic dichroism (which is reflected by the ellipticity of Faraday rotation) one has to include a line broadening for the energy levels, which is assumed to be independent on the spin-splitting in first order ($\Gamma\approx\Gamma_+\approx\Gamma_-$). Formally, line broadening is introduced to Eq. (6) by transforming $E\rightarrow E+i\Gamma$, a procedure already described in Ref. 27, which in turn transforms $\mathrm{Re}[\hat{\varepsilon}_\pm(E)]$ into the complex $\hat{\varepsilon}_\pm(E)$ by analytic continuation to the complex E frame.

Then, Faraday rotation and ellipticity are simultaneously calculated using Eq. (1) and the expressions for the complex dielectric functions $\hat{\varepsilon}_\pm(E)$ for both spin-states, respectively

$$\text{Rotation:}\quad \theta_F(E)=\frac{\omega d}{4nc}\mathrm{Re}[f_+\hat{\varepsilon}_+(E)-f_-\hat{\varepsilon}_-(E)] \tag{8a}$$

$$\text{Ellipticity:}\quad \eta_F(E)=\frac{\omega d}{4nc}\mathrm{Im}[f_+\hat{\varepsilon}_+(E)-f_-\hat{\varepsilon}_-(E)]. \tag{8b}$$

We supplement Eq. (8) by the occupation factors f for the corresponding valence- and conduction-band states, which participate to the transitions $\sigma^\pm$

$$f_+=f_{\sigma^+}^v-f_{\sigma^+}^c \tag{9a}$$

$$f_-=f_{\sigma^-}^v-f_{\sigma^-}^c. \tag{9b}$$

The sign and magnitude of the Faraday rotation depends on band-structure properties: (i) on the joint density of states, (ii) on selection rules for both polarization states, (iii) on the resonance of photon energy with allowed transition energies, and (iv) on the occupation of the participating bands. The rotation spectra can be studied far below the fundamental transition gap ($E\ll E_{\sigma^\pm}$) with a strong reduction of the rotation angle (*nonresonant Faraday rotation*), or near the transition energies ($E\cong E_{\sigma^\pm}$) with a resonant enhancement of the rotation (*resonant Faraday rotation*). The latter should be used to recover spectral features beyond the fundamental absorption edge with a much higher sensitivity than conventional magnetotransmission or reflection experiments. Especially for the nonresonant Faraday effect $E<E_g$, Eq. (6) can be further evaluated for photon energies E not too close to E_g, using the approximations $\Delta E,\Gamma\ll E_g-E$. A Taylor series expansion in terms of $\Delta E,\Gamma$ yields the following approximate expression for the complex dielectric function:

$$\mathrm{Re}[\hat{\varepsilon}_\pm(E)]=C(y)\mp D(y)\frac{\Delta E}{E_g}, \tag{10a}$$

$$\mathrm{Im}[\hat{\varepsilon}_\pm(E)]\approx-\frac{\Gamma_\pm}{E_g}\frac{2A}{\pi y}\left[1-\frac{1}{2y\sqrt{1-y^2}}\times\arctan\left(\frac{2y\sqrt{1-y^2}}{1-2y^2}\right)\right]. \tag{10b}$$

The short notations in Eq. (10a) are

$$y=\frac{E}{E_g}$$

$$C(y)=\varepsilon_\infty-\frac{A\sqrt{1-y^2}}{\pi y}\arctan\left(\frac{2y\sqrt{1-y^2}}{1-2y^2}\right) \tag{11}$$

$$D(y)=\frac{2A}{\pi y\sqrt{1-y^2}}\left[\frac{1}{2}\arctan\left(\frac{2y\sqrt{1-y^2}}{1-2y^2}\right)-y\sqrt{1-y^2}\right]. \tag{12}$$

From these solutions both the Faraday rotation and ellipticity can be calculated, just by taking the differences of the dielectric functions

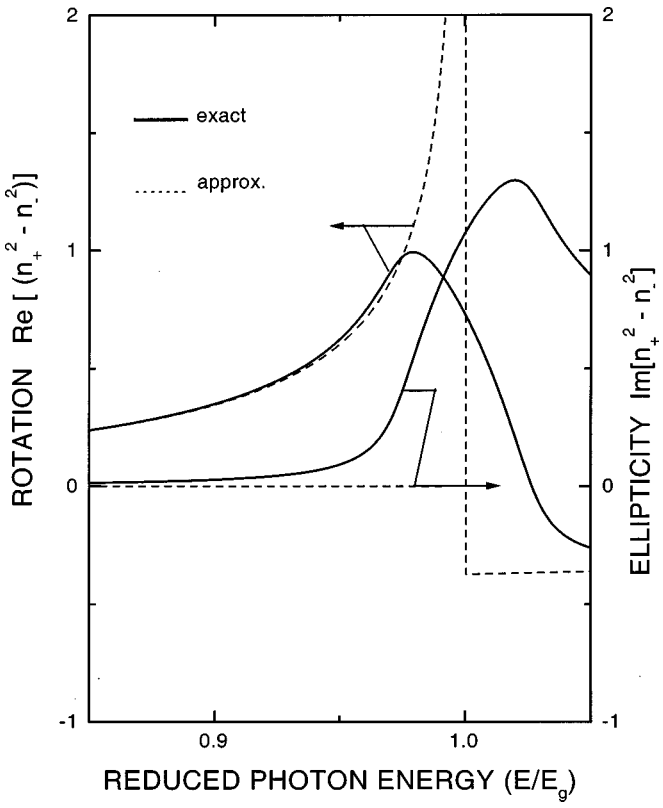

FIG. 1. Interband Faraday rotation and ellipticity as a function of reduced photon energy near the band gap (E_g) of a narrow-gap semiconductor like PbTe. Full lines: Exact calculation for nonparabolic mirrorlike conduction and valence bands, dashed lines: approximations according to Eqs. (13a), and (13b) valid for $E/E_g<1$ and small spin splittings and spin-independent level broadening.

$$\theta_F(E)=\frac{\omega d}{4nc}\left\{(f_+-f_-)C(y)-(f_++f_-)D(y)\frac{\Delta E}{E_g}\right\}, \tag{13a}$$

$$\eta_F(E)=\frac{\omega d}{4nc}\frac{2A}{\pi y}\left[1-\frac{1}{2y\sqrt{1-y^2}}\arctan\left(\frac{2y\sqrt{1-y^2}}{1-2y^2}\right)\right] \times\frac{f_+\Gamma^+-f_-\Gamma^-}{E_g}\approx 0. \tag{13b}$$

Since most of the following magnetooptical experiments are performed for near-band-gap absorption ($y\approx 0.95$), we compare in Fig. 1 the Faraday rotation with ellipticity by plotting $\mathrm{Re}(n_+^2-n_-^2)=\mathrm{Re}(\hat{\varepsilon}_+-\hat{\varepsilon}_-)\propto\theta_F(y)$ and $\mathrm{Im}(n_+^2-n_-^2)=\mathrm{Im}(\hat{\varepsilon}_+-\hat{\varepsilon}_-)\propto\eta_F(y)$ as a function of $y=E/E_g<1$. For photon energies E not too close E_g, the analytical expressions Eq. (13) are shown as dashed lines in comparison with the exact solutions (full lines) of Eq. (8). If we neglect spin-dependent level-broadening ($\Gamma\approx\Gamma_+\approx\Gamma_-$), ellipticity is always an order of magnitude smaller than Faraday rotation, even for $y=0.95$, where $\eta_F(0.95)\approx 0.2\theta_F$. This statement has to be revised, if a spin-dependent imbalance of level broadening is taken into account.

Hence, from inspection of Eq. (13a), the nonresonant Faraday rotation at low-magnetic fields ($f_+\approx f_-$) is linear with ΔE, which is the combined spin splitting in the valence and conduction band, respectively. In a diluted magnetic semiconductor (e.g., $Pb_{1-x}Eu_xTe$) this splitting is mainly caused by the temperature and field-dependent magnetization $M(T,B)$ of the magnetic ions that can be modeled by a phenomenological modified Brillouin function according to Gaj, Planel, and Fishman.[29]

$$\Delta E=g^*\mu_B B+\frac{\alpha_{sf}}{g\mu_B}M(B,T) =g^*\mu_B B+\frac{\alpha_{sf}}{g\mu_B}\left\{g\mu_B Sx(1-x)^{12}N_0 B_s\left(\frac{g\mu_B SB}{k_B(T+T_0)}\right)\right\}, \tag{14}$$

g^* is the effective Lande factor of band electrons in the absence of magnetic ions. The Eu ions enhance the energy splitting by carrier-ion exchange coupling α_{sf}. In a first step, we impose on α_{sf} to be independent on the concentration x, an assumption that has to be revisited later on. In most cases the expression in parenthesis of Eq. (14) ($\alpha_{sf}N_0\approx 0.02$ eV for electrons, ≈ 0.1 eV for holes) (Ref. 30) overwhelmes the first (diamagnetic) part of band electrons. The density of cation sites (Pb+Eu) in $Pb_{1-x}Eu_xTe$ is N_0, of which the portion $x_{\mathrm{eff}}=x(1-x)^{12}$ is occupied by *paramagnetic* Eu-ions ($12=$coordination number of nearest neighbors in a fcc lattice). Due to an antiferromagnetic compensation of Eu spins, the uncoupled active ions ($x_{\mathrm{eff}}N_0$) become more and more diminished for increasing concentration x. $B_s(x)$ is the Brillouin function for $S=\frac{7}{2}$, μ_B and k_B denote the Bohr magneton and the Boltzmann constant, respectively. The temperature parameter T_0 depends in the high-temperature limit ($T\gg T_0$) linearly on the Eu content x (Ref. 9)

$$T_0=\frac{2}{3}S(S+1)xz\frac{J^{ff}}{k_B}=63\frac{2J^{ff}}{k_B}x, \tag{15}$$

J^{ff} is the antiferromagnetic Eu-Eu exchange interaction between nearest neighbors in a fcc lattice ($z=12$). In the limit far below saturation (i.e., for low-magnetic fields), the Brillouin function of Eq. (14) can be expanded for small arguments into the well-known Curie-Weiss law. Hence, the Faraday rotation is linear in B, and the specific rotation (Verdet constant) is derived as

$$V=\frac{1}{d}\frac{\partial\theta_F}{\partial B}\bigg|_{B\to 0}=V_0+\frac{V_M}{k_B(T+T_0)}. \tag{16}$$

V_0 and V_M are constants reflecting the (diamagnetic) background signal and the proportionality between the Faraday rotation and the magnetization, respectively. If ΔE in the Curie-Weiss limit of Eq. (14) is inserted into the expression $\theta_F(E)$ of Eq. (13a), we find ($f_+\approx f_-$)

$$V_0=-\frac{f_++f_-}{4nc\hbar}yD(y)g^*\mu_B \tag{17a}$$

$$V_M=-\frac{f_++f_-}{4nc\hbar}yD(y)\alpha_{fs}N_0\frac{g\mu_B}{3k_B}S(S+1)x(1-x)^{12}. \tag{17b}$$

Apart from the constant Faraday rotation V_0, Eq. (17b) delivers the x dependence of the Verdet constant in the randomly disordered $Pb_{1-x}Eu_xTe$ within the Curie-Weiss approximation ($S=\frac{7}{2}$, $g=2$).

III. EXPERIMENT

A. Setup

The detection of very small Faraday rotation angles ($\approx 10^{-4}$ rad) can be achieved by using differential methods. In our experimental setup a photoelastic modulator (PEM) with a CaF_2 head (transmission range from 200 nm to 8.5 μm) is used to switch the linear polarization of the incident beam between 0° and 90° at a frequency of 114.4 kHz. In front of the detector an analyzer is adjusted to 45° with respect to the incident polarizations. In addition, the light intensity is chopped at about 500 Hz. Due to the large frequency difference of the PEM and of the light chopper, the signal from the detector can be fed into two lock-in amplifiers, which are locked at the reference frequencies of the PEM and light chopper, respectively. If the light reflected or transmitted by the sample remains perfectly linearly polarized, but becomes rotated, from the output of the two lock-in amplifiers the rotation angle is obtained. For small rotation angles and only small ellipticities, the signal depends linearly on the rotation angle and quadratically on the ellipticity, so the detection system is rather insensitive to ellipticity.

The magnetic field- and temperature-dependent magnetooptical experiments were carried out using a split-coil superconducting magnet ($0 \leqslant B \leqslant 7$ T) equipped with a variable temperature insert ($1.6\,\mathrm{K} < T < 300\,\mathrm{K}$). In order to cover the rather wide spectral range for near-band-gap radiation of PbTe (0.190 eV) and EuTe (2.25 eV) we used a 250-W tungsten halogen lamp for the visible to the near infrared part ($\lambda = 500$ nm to 2.5 μm) of the spectrum, and a SiC globar for the midinfrared part ($\lambda = 2.5$ to 8.5 μm) in combination with a single-pass monochromator in front of the polarizer and the PEM.

The magnetization of the epitaxial samples is quantitatively determined by a Quantum Design MPMS-2 SQUID magnetometer in the temperature range of spontaneous antiferromagnetic ordering ($T < T_N = 9.6\,\mathrm{K}$) and in the paramagnetic regime ($T \gg T_N$). Since in the latter case all magnetic ions are released from antiferromagnetic coupling, their absolute concentration can be evaluated using the Curie-Weiss law, as already adopted for the evaluation of the Verdet constant of Eq. (17b). Due to the strong diagmagnetic background signal from the substrate (BaF_2), only a careful (M,T) fit to the observed magnetization data and an accurate determination of the magnetic sample's volume provides a reliable evaluation of the concentration of the magnetic (Eu) ions. The magnetic moment resolution of the magnetometer is 2×10^{-8} emu, which corresponds to 3×10^{11} saturated Eu spins.

B. Samples

$Pb_{1-x}Eu_xTe$ epilayers with Eu contents in the entire concentration range ($0 \leqslant x \leqslant 1$) and thicknesses between 3 and 4.6 μm were deposited on freshly cleaved BaF_2 (111) substrates in a RIBER 1000 molecular-beam epitaxy system equipped with effusion cells for PbTe, Te, and Eu. Prior to the growth of the proper structures, the PbTe and Eu fluxes were calibrated by a quartz crystal microbalance moved to the substrate position. The substrates were preheated in two steps: first at 440 °C for 15 min in the preparation chamber, and then at 580 °C for 30 min in the main chamber. The $Pb_{1-x}Eu_xTe$ samples were grown at a growth rate of 1.1 μm/h and a Te/Eu beam-flux ratio of 2. The substrate temperature was kept at 340 °C and continuous azimuthal rotation during growth ensured a high-lateral homogeneity of both the Eu composition and layer thickness. The growth was monitored by *in situ* reflection high-energy electron diffraction (RHEED) employing a 35 keV electron beam at an incidence angle of 0.3°. The RHEED patterns demonstrate that $Pb_{1-x}Eu_xTe$ nucleates in the form of three dimensional (3D) islands on the substrate, and as the growth proceeds, the islands start to coalesce and merge together to form a smooth 2D surface after about 500-nm layer deposition.

After deposition, the samples were characterized by high-resolution x-ray diffraction in both ω/θ and $\omega/2\theta$ directions. Open detector and triple-axis modes were used for scans of the [222] Bragg reflection. The diffraction patterns exhibit only a single (222) layer peak with a full width at half maximum of the rocking curves increasing from about 65 arcsec for $x=0.02$ to 260 arcsec for $x=0.92$. All samples are single phase, except from the one with nominal content of $x=0.81$. Already, the sample with $x=92$ was definitely single phase.

The values of the Eu content x as given by the flux calibration were compared and found to agree with those obtained by chemical analysis using atomic emission spectroscopy. The free-carrier concentration and mobility have been determined by Hall effect measurements. The conduction is n type in the range of 1.1×10^{17} to $4.4\times10^{17}\,\mathrm{cm}^{-3}$, and the reduction of mobility for increasing x is governed by alloy scattering of carriers in the disordered system.

IV. EXPERIMENTAL RESULTS

In Fig. 2 the Faraday spectra of $Pb_{1-x}Eu_xTe$ epitaxial layers grown on BaF_2 substrate are presented for the concentration range $0 \leqslant x \leqslant 0.52$ at $T=1.8$ K and for $B=6.8$ T. The oscillatory part of the Faraday rotation indicates a Fabry-Perot-like interference caused by multiple reflections at the surface and the BaF_2 substrate interface of the $Pb_{1-x}Eu_xTe$ epitaxial layers. From the envelope of the interference pattern the fundamental absorption edge can be deduced, where the strong asymmetric line shape (due to an increase of the ellipticity for excitation above the energy gap) indicates that the position of the fundamental energy gap is not located at the maximum, but rather at the high-energy side of the spectra. With increasing Eu content an increase of the linewidth, possibly due to the onset of a spin-dependent level-broadening ($\Gamma_+ \neq \Gamma_-$), and a flattening of the Faraday spectra are observed. For samples with an Eu content between $0.6 < x < 0.82$, we were not able to resolve clear signatures for identifying an energy gap. However, samples with an Eu content of $x > 0.8$ showed two resonances in the magnetooptic Kerr reflection (MOKE), see Fig. 3(a). The resonance at 2.25 eV (shown with magnified scale in the inset II) does not change their energetic position for a varying Eu content be-

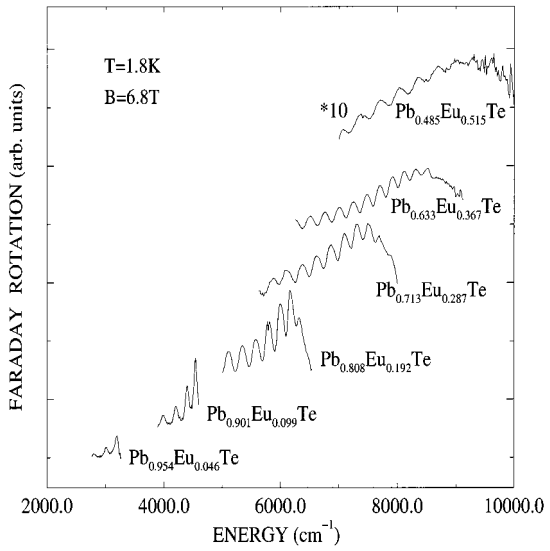

FIG. 2. Experimental traces for Faraday rotation versus photon energy for samples with different Eu-contents.

tween $0.81<x<1$, which indicates that this signature can be attributed to the atomiclike intra-Europium transition between Eu-$4f$ and Eu-$5d$ levels. The second transition energy at 1.42 eV for the $x=0.81$ sample (see insert I) is manifested by a stop of the interference pattern and a point of inflection in the averaged curve, respectively. The appearance of a second transition energy could also be related to the presence of a second phase in this particular sample.[31,32] For comparison, Fig. 3(b) shows a photoreflectance (PR) spectrum with a photometric accuracy $\Delta R/R \approx 10^{-6}$. The fundamental bandgap transition at 1.42 eV is clearly resolved, but this method failed to detect the EuTe-like transition at 2.25 eV in contrast to the MOKE rotation. The broad structure of PR around 1.8 eV is not explained up to now. The occurrence of a signature at 2.25 eV in the MOKE spectrum arises from the enhanced magnetic splitting of a EuTe-related transition, which contributes stronger to MOKE than to reflectance. For comparison a measured transmittance spectrum of the same sample is shown in Fig. 3(c) for two temperatures (5 K, 295 K). The transition between the transparent and absorbing frequency regime is not sharp and does not outline a significant structure at 1.42 eV (see the arrow). We attribute the lack of a sharp absorption edge to a considerable damping of the interband transition due to alloy scattering, which is spin independent. In MOKE this spin-independent parts are cancelled out for the counterrotating waves, and the spectral features of the interband transition are more precisely resolved.

The results on the dependence of the fundamental absorption edge on the Eu content x are summarized in Fig. 4. Three regions with different behavior are characterized by respective linear regression fits.

Figure 5 shows the temperature dependence of the nonresonant Faraday rotation for light excitation below the fundamental energy gap and at a low-magnetic field $B=0.5\,\mathrm{T}$. In the top panel of Fig. 5 the nonresonant Faraday rotation is plotted for EuTe ($x=1$) and $Pb_{1-x}Eu_xTe$ ($x=0.92$) as a function of temperature. As demonstrated in the figure, the cooperative antiferromagnetic phase transition is clearly observed. A series of paramagnetic samples ($0.026 \leqslant x \leqslant 0.367$) is shown in the bottom panel of Fig. 5. A sign

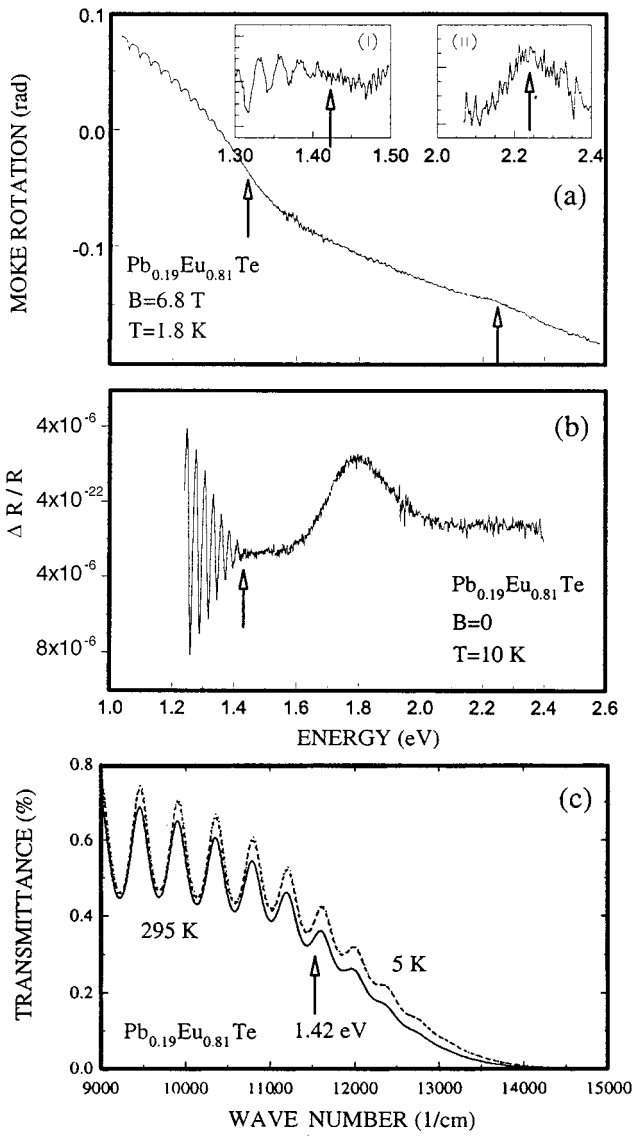

FIG. 3. MOKE rotation (a), photomodulated reflectance $\Delta R/R$ (b) and transmittance (c) as a function of photon energy for $Pb_{1-x}Eu_xTe$ with $x=0.81$. The arrows denote the main absorption features. Inserts: regions around resonances in a magnified scale after subtraction of the average slope. The second EuTe resonance at 2.25 eV (inset II) could not be resolved in the photoreflectance spectrum, in which only the transition at 1.43 eV is observed. The transmission spectra (c) show a rather broad transition region due to alloy scattering, which also obscures the temperature shift of the absorption edge with temperature.

reversal of the nonresonant Faraday rotation is observed for Eu contents between $x=0.1$ and $x=0.367$ in the temperature range below 10 K. This sign reversal is influenced by a residual Faraday rotation of the band electrons of the diamagnetic crystal according to Eq. (17a) neglecting the magnetization of magnetic ions. Therefore, a high-temperature evaluation of the Verdet constant according to Eq. (16) does not lead to unambiguous results for the parameters V_M and T_0. A fit to the modified Brillouin function Eq. (14) down to the lowest temperatures gives more reliable results.

Due to the presence of a magnetic field perpendicular to the sample, spins originally aligned in plane are canted out of plane, which causes an increase of the Verdet constant below

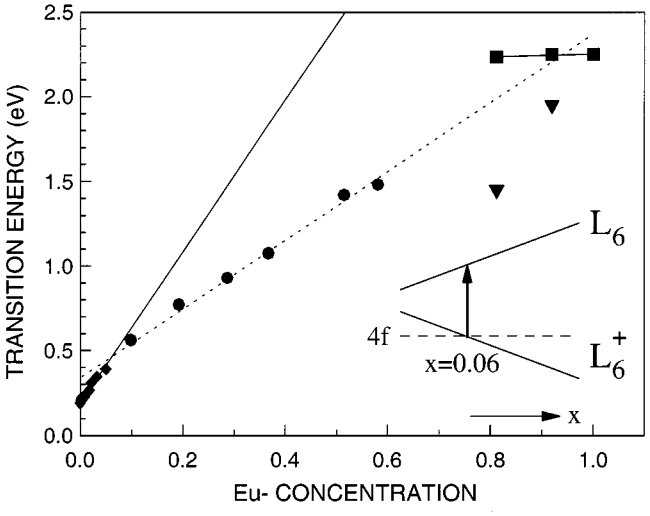

FIG. 4. Experimentally determined transition energies as a function of Eu content with linear regression fits. There are three concentration regimes: (i) ♦: PbTe-like transitions ($x<0.06$), (ii) ●: Eu $4f\rightarrow$PbTe conduction band transitions ($0.06<x<0.80$), (iii) ■: EuTe transitions, ▼: transitions from lower valence bands to $4f$ Eu levels. The insert shows the opening of the gap between PbTe-like bands as a function of Eu content and the $4f$-EuTe reference level.

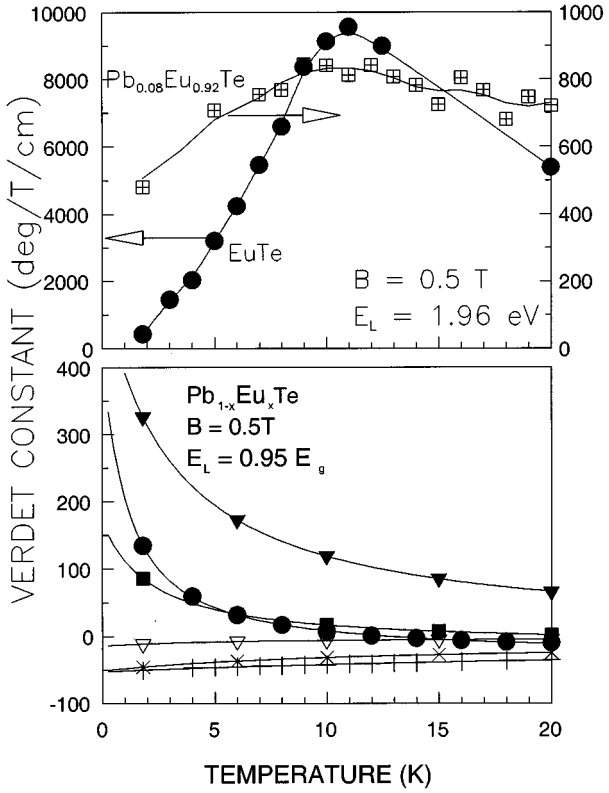

FIG. 5. Temperature dependence of the Verdet's constant at low-magnetic field with photon energies below the fundamental absorption. Upper panel: Antiferromagnetic phase transition for EuTe and $Pb_{1-x}Eu_xTe$ ($x=0.092$). Lower panel: For $Pb_{1-x}Eu_xTe$ with various concentrations in the paramagnetic regime: ●: $x=0.026$, $T_0=0.615$ K; ■: $x=0.046$, $T_0=1.98$ K; ▼: $x=0.1$, $T_0=2.87$ K; ▽: $x=0.192$, $T_0=5.48$ K; ×: $x=0.287$, $T_0=11.21$ K, +: $x=0.367$, $T_0=31$ K. Symbols: experimental data; full curves: modified Brillouin function fits according to Eq. (14).

the Néel point (see Fig. 6). From the figure it is seen, that the Faraday rotation tends to saturate above 6 T, in agreement with published data,[24] which quote for bulk material $B_{\rm sat}=7.2$ T.

We also performed temperature-dependent Hall effect measurements for samples with Eu contents varying from $x=0$ to $x=0.3$. Figures 7(a) and 7(b) show the results of these investigations where the electron concentration [Fig. 7(a)] and mobility [Fig. 7(b)] are plotted as a function of temperature in a magnetic field of $B=0.35$ T. Samples with $x>0.4$ could not be measured because of their high-electrical resistivity caused by the metal-insulator transition (MIT) near $x=0.15$ in these samples.[25] As indicated by the plot of Fig. 7(a) the electron concentration does not vary appreciably on the metallic side of the MIT up to $x=0.15$. Above $x=0.15$ a dramatic decrease of electron concentration, particularly at low temperatures, is observed. It is anticipated that the change of both the carrier concentration and of the mobility in the region of the MIT has also an influence on the magnetooptic spectra.

Figure 8 shows SQUID measurements of the magnetic moment per single Eu atom as a function of temperature for the entire range of Eu contents for an in-plane field of 1 T. The $x=0.01$ sample follows a Curie-Weiss law down to the lowest temperature (2 K). For $x>0.2$ a long-range antiferromagnetic coupling sets in which tends to a cooperative antiferromagnetic phase transition with a well-defined Neél point for the samples with $x>0.8$, as it is marked by the arrows in the inset of the figure. The magnetization of EuTe is not shown in the figure, but practically coincides with the plot for $x=0.90$. The slightly higher Néel point of epitaxial samples ($T_N\approx 10$ K) with respect to $T_N=9.6$ K of a bulk EuTe crystal[15] is caused by residual stresses in the EuTe layer from the BaF_2 substrate. The onset of long-range antiferromagnetic coupling in $Pb_{1-x}Eu_xTe$ coincides with the percolation threshold concentration of $x=0.19$ for a fcc-spin lattice. Figure 9 shows the reciprocal susceptibility in the high-temperature limit ($T\gg T_N$) with a temperature scanning range from 15 up to 250 K and for the same in-plane field of 1 T. As indicated by the insert plot of Fig. 9, the linear fits intersect each other quite close the ordinate axis in a more or less well-defined crossing point. Following the treatment given by Spalek *et al.*,[33] this means that *uncoupled* Eu atoms keep their random distribution even for the highest concentration. This fact is further stressed by the observation, that the paramagnetic Curie temperature ($\Theta_0\approx T_N$, in the high-temperature expansion) scales linearly with concentration: $\Theta(x)=\Theta_0 x$. We remark that the low-field ac susceptibility is independent of frequency of the alternating magnetic field, so that the shoulder observed in the magnetization (Fig. 8) for $x>0.2$ cannot be interpreted as resulting from a spin-glass freezing transition at least for temperatures $T>2.2$ K.

V. DISCUSSION

The transition energies extracted from the resonant Faraday and MOKE rotation spectra of Figs. 2 and 3 are depicted in Fig. 4 as a function of the Eu content for the

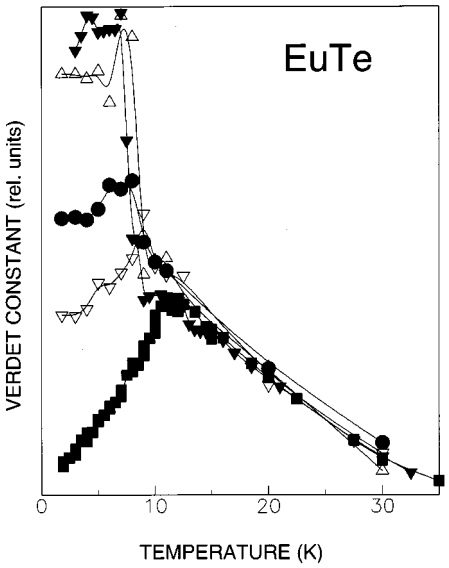

FIG. 6. Verdet's constant of EuTe versus temperature for various perpendicular magnetic fields showing the transition from the antiferromagnetic to the spin-canted phase: ■: $B=0.5$ T; ▽: $B=3$ T; ●: $B=4$ T; △: $B=5$ T; ▼: $B=6$ T.

$Pb_{1-x}Eu_xTe$-system. In the lowest concentration range ($0<x<0.06$, full diamonds in Fig. 4) $Pb_{1-x}Eu_xTe$ has a PbTe-like band structure, and the fundamental transition energy is derived from the PbTe conduction- and valence-band edges, which are located at the L points of the Brillouin zone. A linear regression fit to the data yields[34]

$$E_g(x)=(0.19+4.48\cdot x)\ \text{[eV]}, \quad (0<x\leqslant 0.06). \quad (18)$$

The intercept on the energy axis ($x=0$) represents the low-temperature absorption edge of PbTe (0.19 eV at $T=4.2$ K), and the slope $\partial E_g/\partial x=4.48$ reproduces the published results of earlier works.[7,34,35]

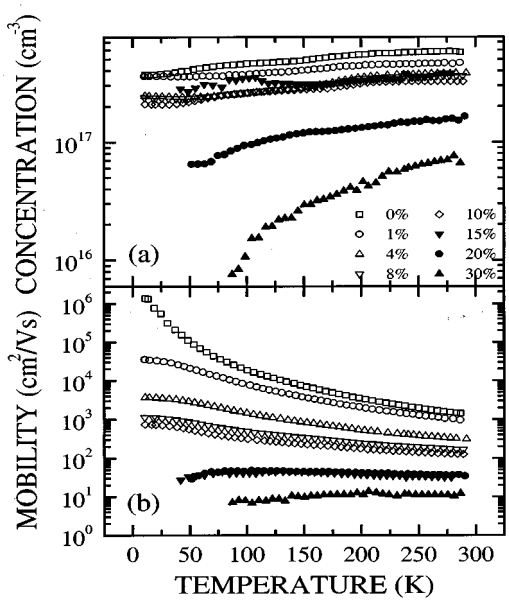

FIG. 7. Carrier concentration (a) and mobility (b) as a function of temperature for $Pb_{1-x}Eu_xTe$ with various concentrations, showing a metal-insulator transition for $0.1<x<0.2$.

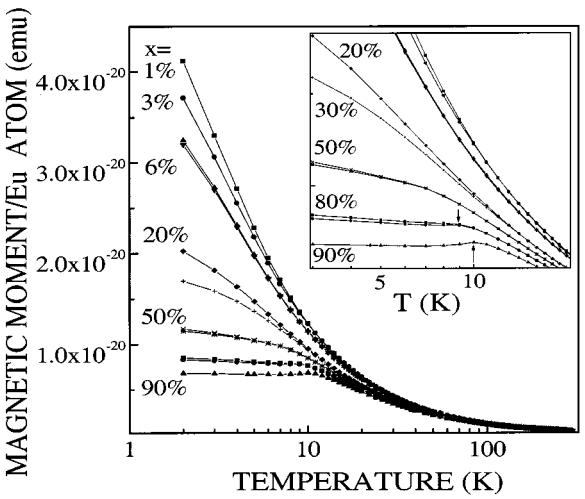

FIG. 8. Magnetic moment per single magnetic ion of $Pb_{1-x}Eu_xTe$ as a function of temperature for an in-plane magnetic field of 1 T and various concentrations, measured by SQUID magnetometry. Insert: Magnified scale showing the antiferromagnetic phase transition (arrows) for the samples $x\geqslant 0.8$. The plot for EuTe ($x=1$) is indistinguishible from the ($x=0.9$) sample.

In the concentration range $0.06<x<0.6$ (full circles in Fig. 4) the energy gap varies in a linear fashion with the Eu content, and *the slope of the x dependence* is *reduced by a factor of two* with respect to Eq. (18). Consequently, we assume that these resonance energies are uniquely associated with a transition from Eu $4f$ levels to the conduction band at the L point of the Brillouin zone of the mixed semiconductor $Pb_{1-x}Eu_xTe$. This fact is explained by the emerging of $4f$ states above the valence-band level of PbTe, i.e., the valence-band edge at the L point of the Brillouin zone is now energetically below the position of the localized Eu-$4f$ levels, which are the initial states of interband transitions. Indeed, since the energetically fixed $4f$ levels take over the role of initial states and the final states of interband transitions remain the L_6^--conduction-band states of PbTe near the

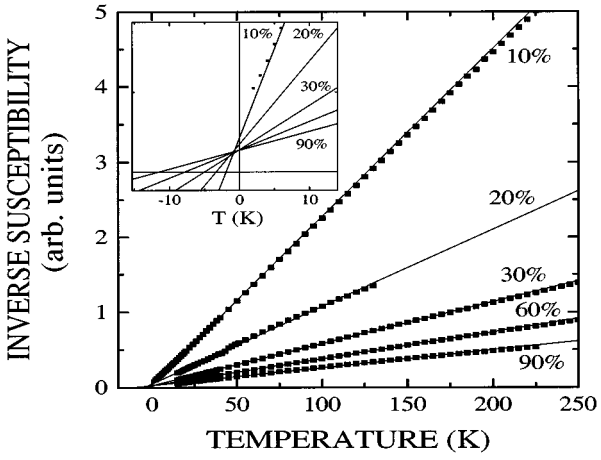

FIG. 9. Reciprocal magnetic susceptibility versus temperature, measured by SQUID magnetometry. Insert: Linear extrapolation to zero and negative temperatures to determine the paramagnetic Curie temperature.

L point of the Brillouin zone, the slope $\partial E_g/\partial x$ is half of that which originally comes from transitions between quasisymmetric valence and conduction bands L_6^+ and L_6^-, both located at the L point of the Brillouin zone. A linear regression to the data yields

$$E_g(x) = (0.34 + 2.03 \cdot x) \ \text{[eV]}, \quad (0.06 < x \leqslant 0.6). \quad (19)$$

From the constant part in Eq. (19) the energetic position of the Eu-$4f$ levels relative to the valence-band edge of the binary PbTe at the L point can be estimated: $\Delta E = 0.34 - 0.19\,\text{eV} = 0.15\,\text{eV}$. It means that the $4f$ level of an isolated paramagnetic Eu ion in the PbTe host lies 0.15 eV below the PbTe valence-band edge. For this estimate we take the $4f$ level of Eu as a reference level. The fixed energetic position of Eu-$4f$ is easily justified by the strong localisation of $4f$-core levels, which are not affected by the delocalization of holes in the PbTe host. For concentrations $x > 0.6$ the resonant interband Faraday rotation due to transitions from the $4f$-Eu levels to the conduction band is no longer observed.

For $x \geqslant 0.81$ two kinds of resonances are observed. The resonance at 2.25 eV (full squares) corresponds to the atomiclike [18,36] internal transition $4f^7(^8S_{7/2}) \rightarrow 4f^6(^7F_J)5dt_{2g}$ of EuTe. The simultaneously observed second transition could be related to electronic transitions from lower $Pb_{1-x}Eu_xTe$ valence bands to empty states above the occupied Eu-$4f$ levels. A second phase of precipitated EuTe as observed by x-ray diffraction could be also taken into account, but the phase separation is not as complete ($<1\%$) as to form a well-established diffraction peak from EuTe precipitates. Furthermore, the small line width of the diffraction peak can only be caused by a perfectly organized mixed crystal. In addition, the temperature-dependent magnetization data (Fig. 8) does not show any discontinuous decrease of the magnetic moment per Eu atom for increasing Eu content.

From the experiments we draw the following conclusions:

(i) The internal EuTe transitions $4f^7(^8S_{7/2}) \rightarrow 4f^6(^7F_J)5dt_{2g}$ as observed at 2.25 eV in the concentration range $0.8 < x \leqslant 1$ are independent from the host crystal PbTe, which means that the onset of a strong *f-d* hybridization of Eu-like orbitals mediates a coupling between adjacent Eu atoms.[18,36] Thus, these x-independent signatures are transitions between localized $4f$ Eu levels and the $5d$-t_{2g} conduction-band states of EuTe, which are delocalized over the full crystal ($x > 0.8$ is well beyond the percolation threshold of $p_c = 0.19$). Interestingly, such a delocalization with a corresponding formation of the EuTe conduction band triggers the onset of a cooperative antiferromagnetic phase transition (see Fig. 8).

(ii) The $4f^6$ levels of Eu atoms are no longer s-like (as the $4f^7$ levels) and experience a strong crystal-field and spin-orbit splitting. The Fermi level is pinned within these split states with partially occupied levels, but also unoccupied ones above the pinned Fermi level. This level acts as a reference level independent of the Eu concentration. Since the $4f$ levels for $x < 0.8$ are highly localized, the carrier transport between them is inhibited [insulator-side of the metal-insulator transition in $Pb_xEu_{1-x}Te$, see Fig. 7(a)]. The empty $4f^6$ levels above the $4f$ reference energy are possibly the final states for excitations from lower-lying valence bands of $Pb_{1-x}Eu_xTe$, which cause the second resonance below 2.25 eV for samples with $x > 0.8$.

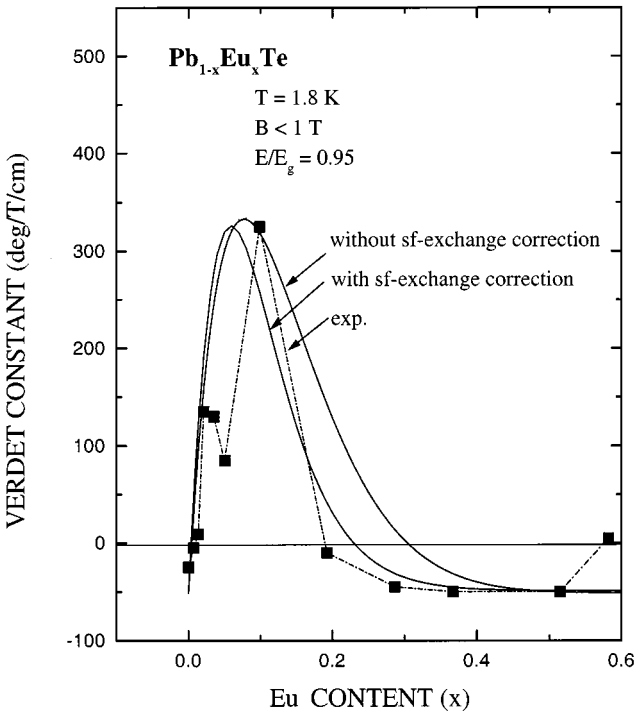

FIG. 10. Theoretical and experimental values of Verdet's constant of $Pb_{1-x}Eu_xTe$ in the concentration range $0 \leqslant x \leqslant 0.6$ for below band-gap excitation ($E/E_g \cong 0.95$). Note the sign reversal at low ($x = 0.01$) and high ($x = 0.2$) concentration. The full curves are calculations taking the *s, p-f* exchange interaction between carriers and Eu-spins as x independent (''without *sf*-exchange correction'') and as x dependent (''with *sf*-exchange correction'') according to Eq. (21).

(iii) The L_6^+ valence-band maximum of PbTe is also lowered with respect of the $4f$ reference level in dependence on the alloy concentration x. The crossover of the PbTe-like L_6^+ valence band with the $4f$ reference level occurs at $x = 0.06$, which is reflected by the change of the slope from 4.48 in Eq. (18) to 2.03 in Eq. (19). If we assume that the L_6^- conduction band of PbTe remains the final state for the photoexcitation process ($x < 0.06$), the opening of the energy gap reflects the x dependence of the positions of the top of the valence band *and* of the bottom of the conduction band. Beyond the crossover of the L_6^+ valence band with the $4f$ Eu levels (for $x > 0.06$) the initial states of photoexcitation are the $4f$ levels, and the final states remain the PbTe L_6^- conduction-band levels. The fact that the slope of the x dependence of the energy gap is reduced by a factor of almost two for $x > 0.06$, as it is observed in the experiment, could be explained that both L_6 conduction and valence bands open as a function of x symmetrically with respect to the reference Eu $4f$ states.

We turn to the analysis of the nonresonant Faraday rotation to relate the magnetooptical data with magnetization detected by the SQUID measurements. In Fig. 10, the Verdet constant is plotted as a function of the Eu content ($x \leqslant 0.6$). The photon energy is always kept below the fundamental energy gap ($E \approx 0.95 E_g, y = 0.95$), and the magnetic

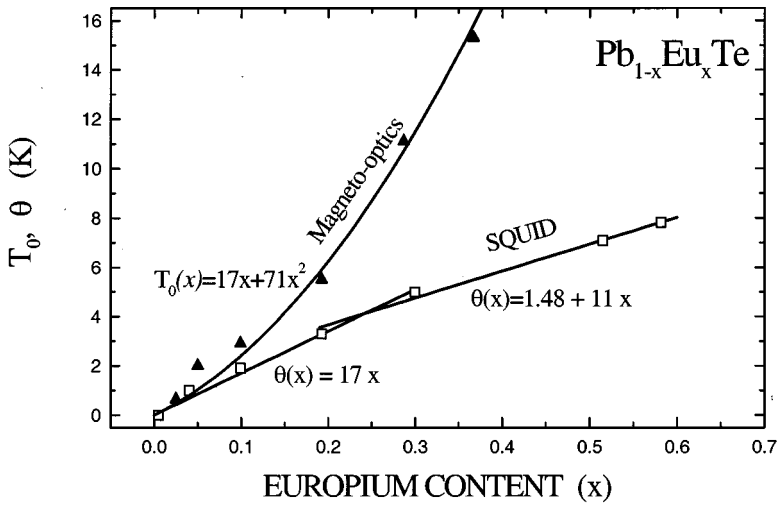

FIG. 11. Paramagnetic Curie temperature determined from a fit to a modified Brillouin function (magneto-optics) and to a Curie-Weiss law (SQUID), respectively. Note the different dependences of MOKE and SQUID data which are related to the metal-insulator transition in $Pb_{1-x}Eu_xTe$ at $x \approx 0.15$.

field was chosen to be small enough (0.5 T) to justify the linear expansion Eq. (13a). In this figure, we compare the experimental Verdet constant (black squares) with the Curie-Weiss approximation given by Eq. (16) taking into account the explicit x dependence $V_M(x)$, as given by Eq. (17b). In one curve (''without *sf*-exchange correction'') we keep the *s,p-f* exchange constant α_{sf} constant, in the second calculated curve (''with *sf*-exchange correction'') we introduce a x-dependent $\alpha_{sf}(x)$. Various concentration ranges with characteristic features are observed. Up to $x=0.15$ Verdet's constant increases more or less monotonically with a corresponding increase of the spin splitting with x. Such a spin splitting is caused by an increase of the magnetization of random paramagnetic centers in a fixed magnetic field

$$\Delta E \propto \alpha_{sf} M(T,B) = \alpha_{sf} x(1-x)^{12} N_0 g \mu_B S B_s\left[\frac{g\mu_B SB}{k_B(T+T_0)}\right]$$
$$\propto \alpha_{sf} x(1-x)^{12}. \tag{20}$$

Due to an enhancement of antiferromagnetic coupling between Eu spins the effective number of paramagnetic spins decreases. If the antiferromagnetic coupling is predominant between nearest neighbors ($z=12$), we calculate a Verdet constant ($x>0.15$) which is larger than that observed in the experiment (curve ''without *sf*-exchange correction''). If we take into account the metal-insulator transition (MIT) at $x>0.15$, as demonstrated by Fig. 7(a) according to which the electron mobility is decreased by orders of magnitude, the stronger deflection of the Verdet constant above $x>0.15$ can be attributed to a x-dependent exchange constant $\alpha_{sf}(x)$

$$\alpha_{sf}(x) = \frac{\alpha_{sf}(x\to 0)}{1+(x/x_c)^2(T_s/T)}. \tag{21}$$

The critical concentration $x_c=0.15$ is related to the MIT. In Fig. 8 of Ref. 25 the temperature dependence of the phase coherence length l_ϕ in the dirty limit ($k_F l_\phi \leqslant 1$) of the metallic phase of $Pb_{1-x}Eu_xTe$ is demonstrated, which is a characteristic length for the backscattering of electrons in the weak-localization limit. If electron-phonon interaction is assumed to be the phase-breaking scattering mechanism, we get $l_\phi = 9.36\times 10^{-7}\ \mathrm{T}^{-3/4}$ close to a reciprocal T dependence. In the cited figure of Ref. 25 a second characteristic temperature for the onset of spin-dependent scattering at $T_s<2$ K is quoted. In this regime the exchange interaction between mobile and localized spins is the dominant phase-breaking mechanism. Hence, the parameter $T_s/T^{3/4} \cong T_s/T$ governs the modification of the carrier-ion exchange α_{sf} due to backscattering of electrons, as long as the concentration of disordered centers lies in the range of the dirty limit ($x>x_c$). We shall demonstrate in the following, that the anticipated formula Eq. (21) is consistent with the observation of the x dependence of the paramagnetic Curie temperature, given in Fig. 11. The x-dependent α_{sf} plays a crucial role for the delicate question why magnetization determined by SQUID may be different from the one from magnetooptics. Recalling Fig. 10, we can fit the experimental data of the Verdet constant much better by introducing $\alpha_{sf}(x)$ from Eq. (21). The curve ''with *sf*-exchange correction'' is calculated by taking $x_c=0.15$, $T=1.8$ K, and $T_s=1.6$ K.

For $x<x_c$ we used the electronic band scheme of PbTe. Therefore, the observed irregularity at $x=0.06$ is not reproduced by our approximate theory. It arises from a change of initial states due to the emergence of Europium $4f$ states at this critical concentration. A sign reversal of the Verdet constant appears at low ($x=0.01$) and high ($x=0.2$) concentrations. We attribute this behavior to a crossover of Faraday rotation between the diamagnetic background (V_0) of band carriers ($g^*=g_c+g_v$) and the magnetization-induced rotation due to localized paramagnetic centers (V_m). Since the Lande factors of electrons g_c and holes g_v differ in sign, we could fit the data of Fig. 10 according to Eqs. (17a,b) with the following set of parameters: $y=0.95$, $g^*=-12$, $f_+ \approx f_- = 0.05$, $\alpha_{sf}(0)N_0 = 0.1$ eV, $T+T_0=4$ K. The values of the Verdet constant in the range $0.81 \leqslant x \leqslant 1$ conincide with those of EuTe and do not depend on x anymore (they are not shown in Fig. 10).

In the composition range $0.2<x<0.50$ the Verdet constant keeps more or less a constant small negative value (V_0). From magnetization data (Fig. 8) a corresponding reduction of the magnetic moment per Eu atom is observed, which demonstrates an increasing antiferromagnetic coupling between individual Eu spins. In the composition range between $0.6<x<0.8$ there is no evidence for a Faraday ro-

tation. A possible explanation is the onset of transitions between lower valence bands of PbTe into the unoccupied $4f$ states above the Fermi level, or just the structural deterioration of samples with higher Eu content. If one takes into account such a transition arising from lower PbTe-like valence bands, then the Faraday rotation of this new transition channel is the reverse of the rotation due to the former transitions from the occupied $4f$ level up to conduction band, if mirrorlike bands with comparable matrix elements and joint density of states are assumed. Formally, this reverse symmetry is taken into account for the calculation of the Faraday rotation by interchanging the role of final and initial states (or just by taking $\Delta E \rightarrow -\Delta E$): This transformation reverses the sign of Faraday rotation of the new transition channel with respect to the former with a corresponding cancellation of the total Faraday rotation. A third alternative interpretation could stem from the assumption that at $x=0.6$ long-range antiferromagnetic order sets in. However, this assumption contradicts the magnetization measurements as well as the temperature dependence of Verdet's constant, where the spontaneous ordering is observed only for $x \geqslant 0.8$ (see insert to Fig. 8).

From modified-Brillouin-function fits to the data presented in the lower panel of Fig. 5 we find a nonlinear dependence of the paramagnetic Curie temperature $T_0(x)$ on the concentration x (see Fig. 11, triangles) in contradiction to magnetization data $\Theta(x)$ from the SQUID. A simple linear fit to the MOKE data (triangles) yields according to Eq. (15) an overestimate for the antiferromagnetic Eu-Eu exchange interaction $2J^{ff}/k_B \approx 0.5\,\mathrm{K}$. In the same figure, the paramagnetic Curie temperature Θ as obtained from SQUID experiments is plotted as a function of x (open squares in Fig. 11). Evidently the SQUID data fit quite close to a linear dependence on x. Using Eq. (15) one finds for the ion-ion exchange integral $2J^{ff}/k_B = 0.27\,\mathrm{K}$ from SQUID data, which is in good agreement with previously published data.[8,10,11] As quoted in Ref. 11, a model that takes into account a single-exchange constant $2J^{ff}$ between *next-nearest* neighbors could explain an increase of $2J^{ff}$ from 0.264 to 0.5 K. However, observations from magnetization steps in high-magnetic field as well as susceptibility measurements contradict this theoretical assumption. Thus, in order to clarify the discrepancy, we introduce our concept of an x-dependent s,p-f exchange interaction $\alpha_{sf}(x)$ from Eq. (21) and make an attempt to find a correlation between the paramagnetic Curie temperatures determined by MOKE and SQUID. Whereas SQUID measures solely the Brillouin function $B_s(y)$ of Eq. (20), magnetooptics is coupled to the product $\alpha_{sf}(x)B_s(y)$. In the Curie-Weiss limit $B_s(y) \rightarrow \mathrm{const}/(T + \Theta_0 x)$ we can calculate

$$\alpha_{sf}(x)B_s(y) \rightarrow \frac{\mathrm{const}}{\left[1+\left(\frac{x}{x_c}\right)^2 \frac{T_s}{T}\right][T+\Theta_0 x]} \approx \frac{\mathrm{const}}{T+\Theta_0 x + T_s\left(\frac{x}{x_c}\right)^2}, \tag{22}$$

Since the Curie-Weiss approximation holds only for $T \gg \Theta_0$, we neglect in Eq. (22) terms of the order $x^3\Theta_0/T$. Therefore, the paramagnetic Curie temperature determined by MOKE differs by an additive quadratic term in x/x_c from $\theta(x)$ determined by the SQUID. Using the data $x_c = 0.15$, $\Theta_0 = 17\,\mathrm{K}$, and $T_s = 1.6\,\mathrm{K}$ from the fit to the Verdet constant (Fig. 10) we could indeed verify the experimental x dependence of the paramagnetic Curie $T_0(x)$ as can be seen from the solid line in Fig. 11 fitted to the triangles. The experimental SQUID data $\Theta(x)$ also show a a slight change of the slope Θ_0 near $x=0.2$. Again we attribute this effect to the onset of MIT for $Pb_{1-x}Eu_xTe$ due to a change of exchange constants between nearest neighbors of Eu spins. The alteration of electron concentration in the conduction band modifies the nearest-neighbor exchange interaction between Eu spins due to a change of the band-mediated (i.e., k-dependent) exchange-polarization[37] between Eu spins. The details of the exchange polarization in $Pb_{1-x}Eu_xTe$ are not investigated up to date.

VI. CONCLUSIONS

The alloy system $Pb_{1-x}Eu_xTe$ has been investigated in the entire concentration range from $x=0$ to $x=1$ by Faraday- and magnetooptical Kerr effect as well as by SQUID magnetometry. The magnetooptical methods provide information on band-structure properties as well as on the magnetic order. Due to the smaller exchange integrals between free carriers and magnetic ions Faraday rotation is not as giant as in Mn-based II-VI semiconductors. The resonant magnetooptical effects have proven that there are three concentration ranges with different types of interband transitions: (i) band-to-band transitions at the L point of the Brillouin zone, representative for the narrow-gap IV-VI semiconductor PbTe ($x<0.06$); (ii) transitions from the localized Eu $4f$ levels to the PbTe-like conduction band ($0.06<x<0.8$); (iii) transitions from localized Eu $4f$ levels to the EuTe-like $5d$ conduction band as well as a second observed transition, which up to now could not be identified unambiguously, but may be due to transitions from lower-lying valence bands up to the $4f$ level, or due to electronic transitions in a $Pb_{1-x}Eu_xTe$ matrix with a lower effective Eu concentration in the case of EuTe precipitates. The variation of the band edges with x was obtained from the data as well as the extrapolated position of the Eu $4f$ levels 150 meV below the PbTe valence-band edge at the L point. At $x=0.06$ a crossover between both states takes place.

To probe the magnetic state, nonresonant Faraday, and Kerr rotation, respectively, have been measured using photon energies about 5% below the fundamental absorption edge. The observed sign reversal of Verdet's constant between $x=0.1$ and $x=0.2$ was explained in terms of a competition between the Faraday rotation of free carriers of the PbTe-like host and that of localized Eu spins. Transport experiments demonstrated a metal-insulator transition in the same concentration range.

The temperature dependence of Verdet's constant can be well described by a modified Brillouin function up to $x<0.4$, which implies a paramagnetic state, in agreement with SQUID magnetometry. Deviations of the paramagnetic Curie temperatures between both experimental methods could be clarified by the postulate that the carrier-ion exchange interaction is x dependent by itself, which governs the magne-

tooptic interactions, but does not primarily influence the magnetization measured by a SQUID. The metal-insulator transition at $x=0.15$ is responsible for the reduction of the carrier-ion exchange interaction.

Both, in Faraday as well as in SQUID measurements a cooperative antiferromagnetic phase transition is found for $x>0.8$. A comparison of magnetooptical and SQUID data demonstrates a good overall agreement, e.g., for the occurrence of a phase transition, but on the other hand remarkable differences exist, owing to characteristic properties of the exchange interaction between free carriers and localized spins.

ACKNOWLEDGMENTS

We thank M. Aigle and S. Holl for their support with the interpretation of data. This work was sponsored by ''Emil-Warburg Stiftung,'' Bayreuth, by the Deutsche Forschungsgemeinschaft (DFG), and by the ''Österreichischer Fonds zur Förderung der wissenschaftlichen Forschung'' (FWF) under Project No. 11 557.

*Present address: Instituto Nacional de Pesquisas Espaciais-INPE, 12200 Sao José dos Campos SP, Brazil.

[1] D. L. Partin, J. Electron. Mater. **13**, 493 (1984).
[2] A. Krost, B. Harbecke, R. Faymonville, H. Schlegel, E. J. Fantner, K. E. Ambrosch, and G. Bauer, J. Phys.: Condens. Matter **18**, 2119 (1985).
[3] M. Tacke, B. Spanger, A. Lambrecht, P. R. Norton, and H. Böttner, Appl. Phys. Lett. **53**, 2260 (1988).
[4] D. L. Partin, IEEE J. Quantum Electron. **QE-24**, 1716 (1988).
[5] D. L. Partin, in *Strained-Layer Superlattices: Materials Science and Technology*, edited by R. K. Williardson and A. C. Beer, Semiconductors and Semimetals (Academic, New York, 1991), Vol. 33, p. 311.
[6] Z. Feit, M. McDonald, R. J. Woods, V. Archambault, and P. Mak, Appl. Phys. Lett. **68**, 738 (1996).
[7] F. Geist, W. Herbst, C. Mejia-Garcia, H. Pascher, R. Rupprecht, Y. Ueta, G. Springholz, G. Bauer, and M. Tacke, Phys. Rev. B **56**, 13 042 (1997).
[8] M. Gorska and J. R. Anderson, Phys. Rev. B **38**, 9120 (1988).
[9] M. Gorska, J. R. Anderson, G. Kido, and Z. Golacki, Solid State Commun. **75**, 363 (1990).
[10] G. Braunstein, G. Dresselhaus, J. Heremans, and D. Partin, Phys. Rev. B **35**, 1969 (1987).
[11] E. ter Haar, V. Bindilatti, N. F. Oliveira, Jr., G. H. McCabe, Y. Shapira, Z. Golacki, S. Charar, M. Averous, and E. J. McNiff, Jr., Phys. Rev. B **56**, 8912 (1997).
[12] G. Bauer, in *Narrow Gap Semiconductors, Physics and Applications*, edited by Wl. Zawadzki, Lecture Notes in Physics Vol. 133 (Springer, Berlin, 1980), p. 427.
[13] H. Pascher, Appl. Phys. **34**, 107 (1984).
[14] R. B. Dennis, Ph.D. thesis, University of Reading, 1969.
[15] N. F. Oliveira, Jr., S. Foner, Y. Shapira, and T. B. Reed, Phys. Rev. B **5**, 2634 (1972).
[16] J. Vitins and P. Wachter, Phys. Rev. B **12**, 3829 (1975).
[17] P. Wachter, CRC Crit. Rev. Solid State Sci. **3**, 189 (1972).
[18] J. Schoenes, Z. Phys. B **20**, 345 (1975).
[19] J. Schoenes and P. Wachter, Physica B **86-88**, 125 (1977).
[20] S. J. Cho, Phys. Rev. B **1**, 4589 (1970).
[21] R. M. Nowotny and K. Binder, Z. Phys. B **77**, 287 (1989).
[22] P. Wachter, in *Handbook on the Physics and Chemistry of Rare Earths*, edited by K. A. Gschneidner and L. Eyring (North-Holland, Amsterdam, 1979), p. 507.
[23] A. Mauger and C. Godart, Phys. Rep. **141**, 51 (1986).
[24] H. Hori, R. Akimoto, M. Kobayashi, S. Miyamoto, M. Furusawa, N. Kreines, A. Yamagishi, and M. Date, Physica B **201**, 438 (1994).
[25] A. Prinz, G. Brunthaler, Y. Ueta, G. Springholz, G. Bauer, G. Grabecki, and T. Dietl, Phys. Rev. B **59**, 12 983 (1999).
[26] D. U. Bartholomew, J. K. Furdyna, and A. K. Ramdas, Phys. Rev. B **34**, 6943 (1986).
[27] H. Krenn, S. Yuan, N. Frank, and G. Bauer, Phys. Rev. B **57**, 2393 (1998).
[28] S. Yuan, H. Krenn, G. Springholz, and G. Bauer, Phys. Rev. B **47**, 7213 (1993).
[29] J. Gaj, R. Planel, and G. Fishman, Solid State Commun. **29**, 435 (1979).
[30] H. Krenn, Phys. Scr. **T45**, 219 (1992).
[31] L. Salamanca-Young, S. Nahm, M. Wuttig, D. L. Partin, and J. Heremans, Phys. Rev. B **39**, 10 995 (1989).
[32] L. Salamanca-Young, D. L. Partin, and J. Heremans, J. Appl. Phys. **63**, 1504 (1988).
[33] J. Spalek, A. Lewicki, Z. Tarnawski, J. K. Furdyna, R. R. Galazka, and Z. Obuszko, Phys. Rev. B **33**, 3407 (1986).
[34] S. Yuan, H. Krenn, G. Springholz, Y. Ueta, and G. Bauer, Phys. Rev. B **55**, 4607 (1997).
[35] A. Ishida, S. Matsuura, M. Mizuno, Y. Sase, and H. Fujiyasu, J. Appl. Phys. **63**, 4572 (1988).
[36] T. Kasuya, CRC Crit. Rev. Solid State Sci. **3**, 131 (1972).
[37] L. Liu, Phys. Rev. B **26**, 975 (1982).